Ultra-wideband Microstrip Patch Antenna with Artificial Magnetic Conductor and Nearly Constant Radiation Pattern for Breast Tumor Detection

Ali Raza, Maryam Liaqat, Vinicius M. Pepino and Ben-Hur Viana Borges

Abstract— **This letter presents the design, fabrication, and characterization of an ultra-wideband (UWB) microstrip patch antenna engineered for the early detection of breast tumors. The proposed design offers a nearly constant radiation pattern, high gain, and compact size through the utilization of an artificial magnetic conductor (AMC) structure comprising four different unit cells. This design feature ensures uniform coverage and reception across breast tissue, critical for early-stage tumor detection. Operating in the 2.9 GHz to 7.0 GHz frequency band, the antenna integrates a back-plane reflector that helps increasing the gain by 3 dB while enhancing bandwidth at low frequencies, thereby improving directivity and front-to-back ratio. The proposed antenna achieves a peak gain of ~8.1 dBi with the AMC. Furthermore, our antenna exhibits a nearly constant radiation pattern across 93% of its operating bandwidth. These characteristics highlight the antenna suitability for applications such as diagnosis of breast carcinoma and microwave imaging.**

Index Terms—**Breast Cancer, Microwave Imaging, wideband Antenna, metamaterial, radiation pattern.**

I. INTRODUCTION

BREAST cancer is considered as the most life-threatening cancer among the female population [1-4], with projections indicating approximately 1.9 million new cases diagnosed globally each year [5, 6]. Conventional imaging techniques, including X-ray mammography, Magnetic Resonance Imaging (MRI), Computed Tomography (CT), ultrasound, and nuclear medicine imaging are usually employed for breast cancer detection [4]. However, these techniques have limitations, such as missed detections, false positives and negatives, ionizing radiation, higher costs, complex operation, or low resolution [1]. In recent years, microwave imaging (MWI) systems have emerged as a promising technique for early breast cancer diagnosis, exploiting the substantial contrast between the dielectric properties of normal and malignant tissues [9, 10]. Notably, MWI systems are non-ionizing, cost-effective, compact, comfortable for patients, and able to detect small size tumors with very low power density and high resolution [10-13].

In this context, microwave antennas play a pivotal role in MWI systems because they are used for transmitting the signal into the breast tissue and for detecting the scattered electromagnetic field by the tumor that will later be transformed into three-dimensional images. Several antenna parameters affect image reconstruction, including size, bandwidth, radiation efficiency, as well as the flatness of both gain and radiation pattern over the operating bandwidth [12]. Ultra-wideband (UWB) operation is especially advantageous in imaging applications due to its ability to generate high-resolution images and achieve precise tumor detection and localization [14]. This is because higher frequencies offer finer detail but have shallower penetration into breast tissues, while lower frequencies provide deeper penetration but lower resolution [15]. In addition, UWB antennas typically offer a bandwidth exceeding 20% relative to their center frequency, featuring either directional or omnidirectional radiation patterns tailored to specific applications [5, 12, 13, 16]. However, these antennas often suffer from low radiation efficiency and limited gain (< 5 dBi). To address this challenge, various techniques have been employed to enhance the performance of microstrip patch antennas, focusing on improving gain, efficiency, directivity, and bandwidth. Different approaches including the utilization of cross-Vivaldi antennas [1], unit cell antennas [2], metal-backed artificial magnetic conductors (AMCs) [3, 17], metamaterial (MTM) antennas [18], and slot-loaded antennas [5]. Remarkably, array reflectors based on AMC technology are recognized for enhancing both the gain and bandwidth of patch antennas [1-3].

Building upon the previous discussion, this letter presents three major contributions: first, a compact UWB antenna design with a standard FR4 substrate; second, the proposal of utilizing a metamaterial AMC structure with four different unit cells; and lastly, design techniques aimed at enhancing antenna performance in terms of gain, directivity, and bandwidth, while maintaining an approximately constant radiation pattern over 93% of the entire bandwidth.

This letter is organized as follows: firstly, in Section II, we present the design and simulation procedures of the AMC unit cells and patch antenna. Then, in Section III, we demonstrate the simulated and experimental characterization, including the nearly constant radiation pattern of the proposed antenna with and without the AMC. Finally, we provide some concluding remarks in Section IV.

Ali Raza (email: aliraza@usp.br), Vinicius M. Pepino (email: vinicius.pepino@usp.br), and Ben-Hur V. Borges (email: benhur@sc.usp.br) are with the University of São Paulo, Campus São Carlos, SP, CEP 13566-590, São Carlos, SP, Brazil. Maryam Liaqat (email: drmaryam.liaqat@uo.edu.pk) is with the University of Okara, Okara, Pakistan.

II. DESIGN METHODOLOGY OF THE PROPOSED ANTENNA

The main goal of using a UWB patch antenna with an AMC is to achieve directive radiation (high gain), wide bandwidth, and high radiation efficiency across its entire frequency range. Thus, ANSYS High Frequency Structure Simulator (HFSS) 2022 R2 [19] is used to optimize the antenna, which is later fabricated by an LPKF ProtoMat S103 circuit prototyper. The designing and characterization procedure are as follows.

A. Metamaterial Unit Cell and AMC Layout Design

The primary objective is to design unit cells (we chose four different cells to fit in the available area) that ensure reflection within a 3 GHz to 10 GHz range, typical for MWI applications [1, 3]. The basic design of each unit cell is depicted in Fig. 1 (a), with their geometric parameters listed in Table 1. The overall AMC structure size is 46.5×42 mm^2. Each individual unit cell consists of two squared concentric copper rings on a FR4 substrate, as depicted in Figs. 1(a) and (b). The parameters of the unit cells are obtained through optimization routines and adjusted according to the antenna frequency response. The arrangement of the unit cells is designed to maintain a nearly constant radiation pattern across the bandwidth of the antenna. Various combinations of unit cells were investigated during the optimization process. Ultimately, the configuration with four distinct unit cells in each column (as depicted in Fig. 1 (b)) exhibited optimal performance. The remaining dimensions of the proposed AMC structure are as follows: $X = 46.5$ mm, $Y = 42$ mm, $T_1 = 14$ mm, $S_1 = 1.5$ mm, and $S_4 = 2.4$ mm. The simulated S_{11} of each individual unit cell is shown in Fig.1(c), while the inset shows the fabricated structure.

TABLE I
OPTIMIZED PARAMETERS OF EACH PROPOSED UNIT CELL

Para.	1st unit cell Size (mm)	2nd unit cell Size (mm)	3rd unit cell Size (mm)	4th unit cell Size (mm)
U	16.0	16.0	12.0	8.0
L_1	11.0	12.0	5.8	5.7
L_2	7.50	6.20	3.85	3.50
W_1	11.0	12.0	5.8	5.7
W_2	2.0	2.4	1.0	1.0
W_3	0.80	0.50	0.60	0.25
W_4	0.70	2.40	0.35	0.70
W_5	7.50	6.20	3.85	3.50

B. Patch Antenna Design Optimization

The design of the proposed UWB antenna follows three-step procedure, illustrated in Fig. 2. During the optimization process, we vary the dimensions of the ground plane length (G_L), the side reflectors (B_L, B_W), and the notched regions (A_W, A_L, C_L) on the patch. In the first step, we design a rectangular-shaped patch antenna (R_W, R_L) with a full ground plane, as shown in (a). Next, we create an indentation (notch) on the top of the antenna to enhance its bandwidth and incorporate two side reflectors to control the radiation pattern. Finally, on the bottom surface of the substrate, we define a partial ground plane, as depicted in (b). In the final refinement step, we remove excess material surrounding the central patch, near the feedline (F_W, F_L), and ground plane, as shown in Fig. 2(c).

The simulated S_{11} of the design steps illustrated in Fig. 2 are shown in Fig. 3(a). The impact of various antenna parameters, including the notched region around the central patch, the length of side reflectors, and the ground plane, is shown in Figs. 3(b)-(d). As shown in (a, dashed blue lines), the impedance is mismatched for frequencies below 9.3 GHz, but it exhibits a narrow resonance at 9.5 GHz with a return loss S_{11} = -27dB. Antenna (b) shows wideband operation between 4 GHz and 8.7 GHz, with a minimum return loss of -22 dB at the resonance of 6.46 GHz, as shown in (a, dashed red lines). It is noteworthy that the design of antenna (c) shifted towards lower frequencies, now covering the range from 2.8 GHz to 7.3 GHz, with a
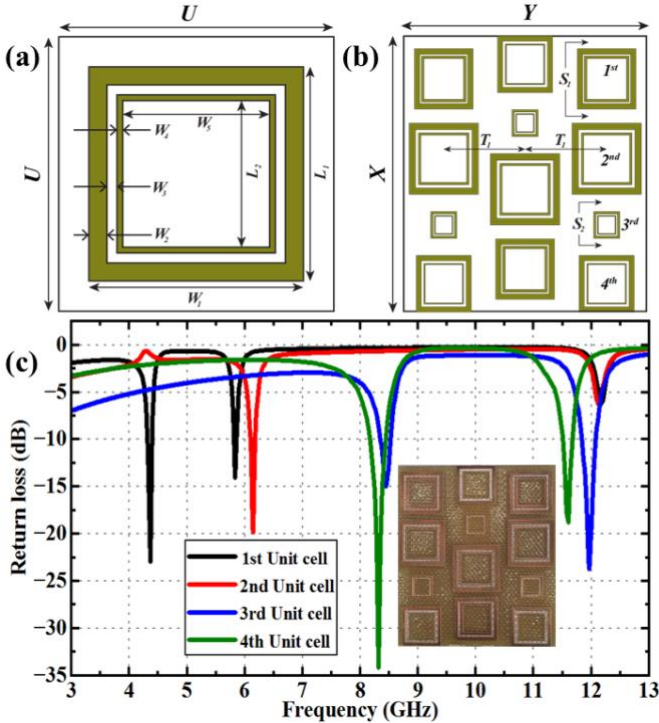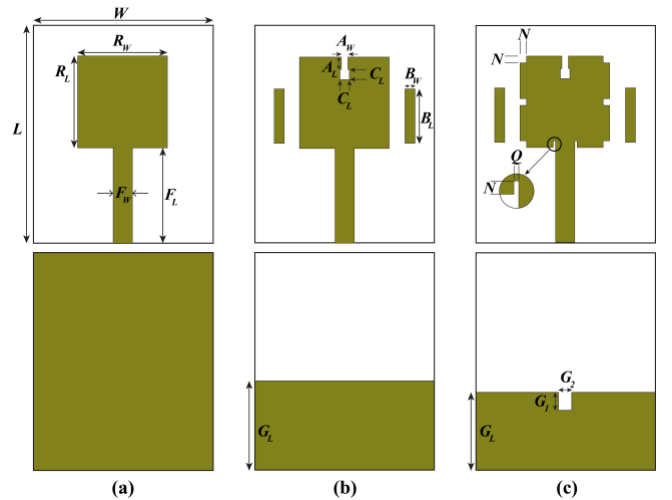

Fig. 1. (a) Top view of the unit cell. (b) Arrangement of three columns for the AMC structure design with four unit cells each. (c) Simulated reflection coefficient (S_{11}) of each unit cell in the 3-10 GHz range. The inset shows the fabricated AMC.

Fig. 2. Evolution process of antenna front (top row) and back (bottom row) view design at different steps (a,b,c). In (b), the ground plane length G_L = 14 mm. The optimized antenna design is shown in (c), with all parameters listed in Table II.

TABLE II
OPTIMIZED PARAMETERS OF THE ANTENNA IN FIG. 2(C).

Para meter	Value (mm)	Para meter	Value (mm)	Para meter	Value (mm)	Para meter	Value (mm)
L	34.00	W	28.00	A_L	2.00	A_W	1.00
R_L	14.25	R_W	13.90	C_L	1.50	N	1.00
F_L	14.78	F_W	3.00	Q	0.50	G_2	1.70
B_L	8.50	B_W	1.50	G_L	12.60	G_1	3.00

minimum return loss of -25 dB at 5.2 GHz. Moreover, reducing the size of the ground plane and incorporating notches in the antenna helped expand the S_{11} bandwidth but caused a shift of the resonance frequency towards lower values, as depicted in (a). The final proposed antenna in (c) features a partial ground plane to achieve high gain, compact size, and large bandwidth.

III. RESULTS AND DISCUSSION

This section describes the experimental characterization of the antenna and AMC structure fabricated on an FR4 substrate (1.6 mm thick, $\varepsilon_r = 4.1$ and $\tan\delta = 0.02$). The measured S_{11} curves are obtained using a vector network analyzer (VNA, Rohde & Schwarz ZVA-40, 10 MHz – 40 GHz).

A. Proposed Antenna without AMC

Figure 4 shows the simulated and measured return loss (a) and peak realized gain (b), respectively, both without the AMC, as function of frequency for the optimized antenna. The front and backside of the fabricated antenna are shown as insets in (a). The measured bandwidth ($S_{11} < $ -10 dB) is 3.6 GHz, with minimum return loss (-24 dB) at 4.95 GHz, while the maximum measured gain is 5.2 dBi at 6.4 GHz, with both showing good agreement with the numerical analysis.

B. Integration of the AMC structure with the Antenna

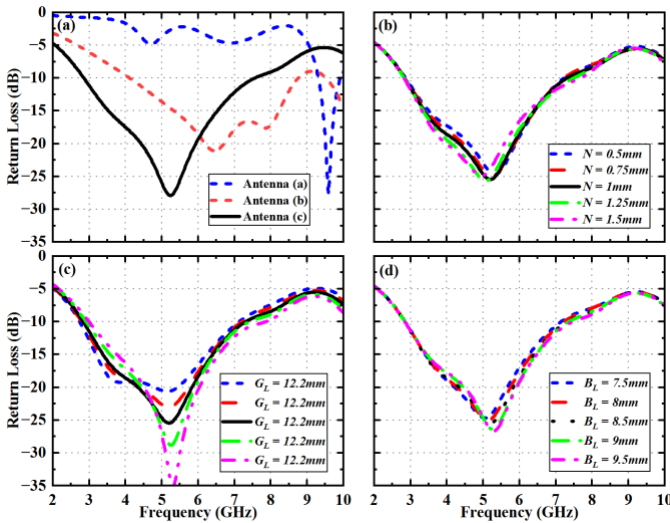The measurement setup and top view of the fabricated antenna integrated with the AMC structure are depicted in Figs.

Fig. 3. (a) Simulated reflection coefficient of the three antenna designs; the -10 dB bandwidth of the proposed antenna is 4.5 GHz (2.8 GHz - 7.3 GHz). (b)-(d) show the frequency response for variations of the notched region (N), ground plane length (G_L), and backplane length (B_L), respectively.
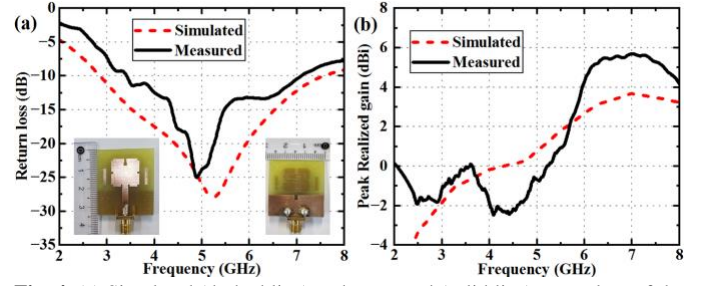

Fig. 4. (a) Simulated (dashed line) and measured (solid line) return loss of the antenna without the AMC. The difference between the simulated and measured bandwidth of the antenna is 0.7 GHz. Inset shows front and back planes of the fabricated antenna. (b) Simulated (dashed line) and measured (solid line) peak realized gain, with a gain difference of 2 dB at 6.4 GHz.

5(a) and (b). The gap between the antenna and the AMC is 15mm. The measured and simulated S_{11} curves of the antenna are shown in Fig. 6(a). The simulated bandwidth of the antenna with the reflector is 4.4 GHz, covering a range from 2.6 GHz to 7 GHz, with a minimum S_{11} of -26 dB at 4 GHz. However, the measured bandwidth is 4.1 GHz, ranging from 2.9 GHz to 7 GHz with a resonance at approximately 4.6 GHz. When the AMC is employed as the backplane reflector of the antenna, the bandwidth increases by 0.5 GHz, and the resonance shifts to 4.6 GHz, as shown in Fig. 6(b). Differences between simulated and measured results are primarily due to fabrication imperfections and substrate permittivity differences. The lowest measured return loss occurs at approximately 4.6 GHz with a value of -31 dB. The first resonance frequency is blueshifted by approximately 1 GHz across the bandwidth when compared to the simulated S_{11}, as illustrated in Fig. 6(a).

Utilizing the AMC backplane results in a significant increase in gain while also expanding the bandwidth, as shown in Fig. 6(a). The maximum simulated gain with the AMC is 6.5 dBi at 5.3 GHz, and the maximum measured gain is approximately 8.1 dBi at 6.47 GHz. Compared to the antenna without the AMC (see Fig. 6(b)), the AMC increases the maximum measured gain by approximately 3 dB. With the AMC, most of the radiated power is directed towards the top side instead of both sides, thereby enhancing the gain while maintaining a nearly constant radiation pattern over the bandwidth.

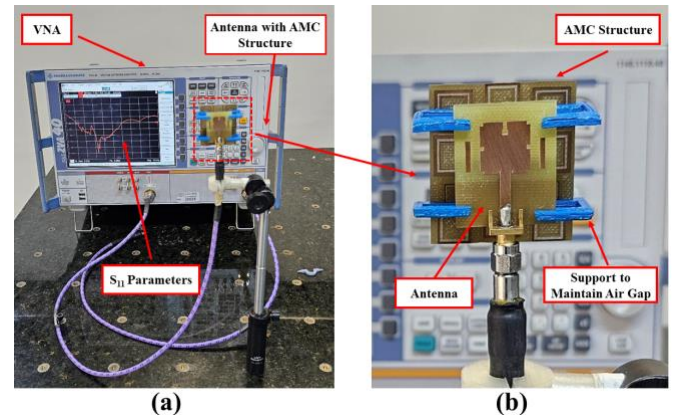To clarify the antenna radiation performance, the radiation

Fig. 5. (a) Experimental setup of the antenna with reflector. (b) Front view of the antenna with the AMC structure. The gap between antenna and reflector is 15 mm, maintained by using 3D-printed support with Acrylonitrile Butadiene Styrene (ABS) material, with relative permittivity $\varepsilon_r = 2.7$.
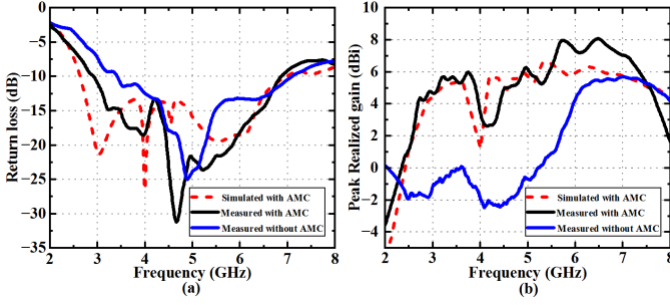
Fig. 6. (a) Return loss and (b) peak realized gain as function of frequency, with dashed lines representing simulated results and solid lines measured data, without (blue solid line) and with AMC (black solid line). Both figures show the measured results without the AMC for the sake of comparison.

pattern in the azimuth plane of the antenna without and with the AMC structure is illustrated in Figs. 7(a)-(d) at (a) 3.8 GHz, (b) 4.56 GHz, (c) 6.25 GHz, and (d) 7 GHz. It is noteworthy that the reflector reduces the backscattered signal, thereby increasing the front-to-back ratio. Additionally, observe how the radiation pattern shape remains nearly constant at all frequencies, which is of significant importance for MWI applications. The correlation coefficient of the measured radiation pattern over the bandwidth is present in Fig. 7(e) (smoothed using a gaussian average function). The correlation coefficient is above 80% in 93% of the antenna bandwidth. The
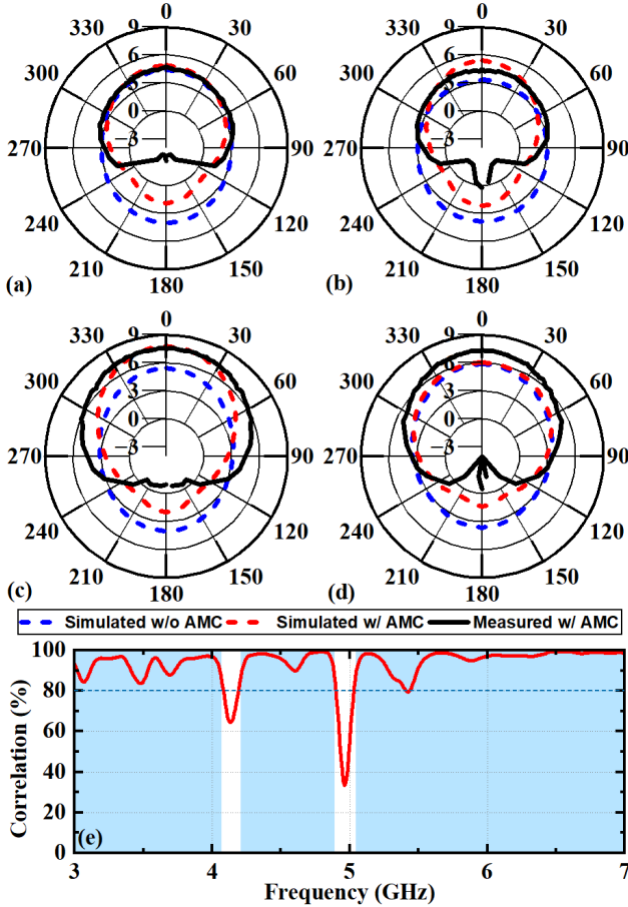

Fig. 7. Simulated and measured radiation pattern (azimuth plane) with and without the AMC structure at (a) 3.8 (b) 4.56 (c) 6.25 and (d) 7 GHz. (e) Correlation coefficient of the radiation patterns with respect to 6.47 GHz (highest gain frequency). Note that the correlation is above 80% (dashed line) in 93% of the whole bandwidth (highlighted by blue regions).
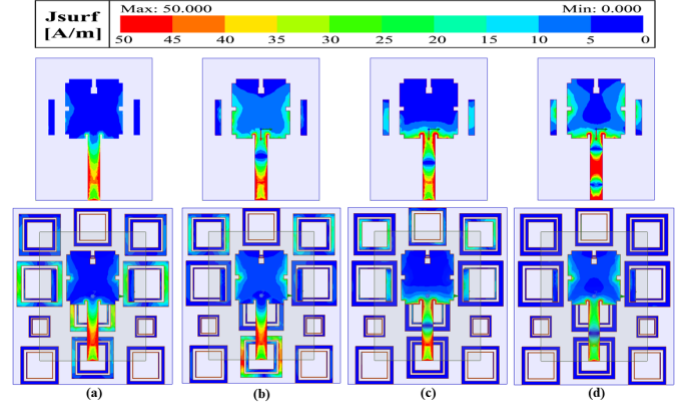

Fig. 8. Surface current distribution obtained without (top row) and with (bottom row) the AMC at (a) 3.8 GHz, (b) 4.56 GHz, (c) 6.25 GHz and (d) 7 GHz. The patch antenna and AMC are separated by 15 mm, but the current density is superposed for clarity.

TABLE III
COMPARISON OF DIFFERENT UWB ANTENNAS DESIGN WITH PROPOSED ONE IN TERMS OF VARIOUS FEATURES

Ref.	Dimension (mm²)	Material	Operating Frequency Range (GHz)	Gain (dBi)	Published Year
[1]	60.0 × 77.7	Rogers RT5880	2.7 - 10.2	9.3	2019
[5]	29.0 × 26.6	Rogers RT5880	3.8 - 10.1	6.8	2023
[3]	76.0 × 44.0	FR4	3.0 - 7.6	10.0	2018
[7]	40.0 × 40.0	FR4	2.5 - 11	7.2	2019
[8]	26.4 × 44.1	F4B	1.3 - 11.6	5.0	2022
This work	28.0 × 34.0	FR4	2.9 - 7	8.1	2024

surface current distribution without and with the AMC is shown in Figs. 8(a)-(d) for frequencies of 3.8 GHz (a), 4.56 GHz (b), 6.25 GHz (c) and 7 GHz (d). The current is concentrated around the feedline and the larger unit cells. Table III compares our proposed antenna with other recent works. It is worth noting that our work achieves ultra-wideband with high gain in a more compact size compared to similar antennas using a low-cost FR4 substrate.

IV. CONCLUSION

In summary, we have successfully designed and fabricated a UWB antenna with an AMC structure for operation between 2.9 GHz and 7 GHz. The proposed antenna, along with the four-type cell AMC reflector, achieved high gain and a nearly constant directive radiation pattern. The back-plane AMC effectively suppressed backscattering and increased the antenna gain by 3 dB. Our antenna exhibits a measured bandwidth of 4.1 GHz, with a minimum return loss at approximately 4.6 GHz and a maximum gain of 8.1 dBi. The measured results demonstrate that the integration of the reflector with the antenna enhanced gain, directivity, and controlled radiation characteristics, while maintaining a nearly constant radiation pattern profile across 93% of its operating bandwidth. These results establish our proposed antenna with AMC structure as a strong candidate for MWI applications.

REFERENCES

[1] M. T. Islam, M. Samsuzzaman, S. Kibria, N. Misran, and M. T. Islam, "Metasurface loaded high gain antenna based microwave imaging using

iteratively corrected delay multiply and sum algorithm," *Scientific reports,* vol. 9, no. 1, p. 17317, 2019.

[2] M. Slimi, B. Jmai, H. Dinis, A. Gharsallah, and P. M. Mendes, "Metamaterial Vivaldi antenna array for breast cancer detection," *Sensors,* vol. 22, no. 10, p. 3945, 2022.

[3] M. Z. Mahmud, M. T. Islam, N. Misran, S. Kibria, and M. Samsuzzaman, "Microwave imaging for breast tumor detection using uniplanar AMC based CPW-fed microstrip antenna," *IEEE Access,* vol. 6, pp. 44763-44775, 2018.

[4] A. Syed, N. Sobahi, M. Sheikh, R. Mittra, and H. Rmili, "Modified 16-quasi log periodic antenna array for microwave imaging of breast cancer detection," *Applied Sciences,* vol. 12, no. 1, p. 147, 2021.

[5] F.-e. Zerrad *et al.*, "Microwave Imaging Approach for Breast Cancer Detection Using a Tapered Slot Antenna Loaded with Parasitic Components," *Materials,* vol. 16, no. 4, p. 1496, 2023.

[6] R. L. Siegel, K. D. Miller, H. E. Fuchs, and A. Jemal, "Cancer statistics, 2022," *CA: A Cancer Journal for Clinicians,* vol. 72, no. 1, pp. 7-33, 2022.

[7] S. Kibria, M. Samsuzzaman, M. T. Islam, M. Z. Mahmud, N. Misran, and M. T. Islam, "Breast phantom imaging using iteratively corrected coherence factor delay and sum," *IEEE Access,* vol. 7, pp. 40822-40832, 2019.

[8] Z. Chao, Z. Zitong, X. Pei, Y. Jie, L. Zhu, and L. Gaosheng, "A miniaturized microstrip antenna with tunable double band-notched characteristics for UWB applications," *Scientific Reports,* vol. 12, no. 1, p. 19703, 2022.

[9] D. Bhargava and P. Rattanadecho, "Microwave imaging of breast cancer: Simulation analysis of SAR and temperature in tumors for different age and type," *Case Studies in Thermal Engineering,* vol. 31, p. 101843, 2022.

[10] M. LIAQAT, "Development of flexible microwave antennas for breast cancer imaging system," 2018.

[11] D. N. Elsheakh, R. A. Mohamed, O. M. Fahmy, K. Ezzat, and A. R. Eldamak, "Complete breast cancer detection and monitoring system by using microwave textile based antenna sensors," *Biosensors,* vol. 13, no. 1, p. 87, 2023.

[12] A. M. Qashlan, R. W. Aldhaheri, and K. H. Alharbi, "A Modified Compact Flexible Vivaldi Antenna Array Design for Microwave Breast Cancer Detection," *Applied Sciences,* vol. 12, no. 10, p. 4908, 2022.

[13] K. Hossain, T. Sabapathy, M. Jusoh, S.-H. Lee, K. S. A. Rahman, and M. R. Kamarudin, "Negative Index Metamaterial-Based Frequency-Reconfigurable Textile CPW Antenna for Microwave Imaging of Breast Cancer," *Sensors,* vol. 22, no. 4, p. 1626, 2022.

[14] N. V. Shahmirzadi, V. Tyagi, J. Nguyen, R. Kazemivala, N. K. Nikolova, and C.-H. Chen, "Planar array of UWB active slot antennas for microwave imaging of the breast," *IEEE Transactions on Antennas and Propagation,* vol. 71, no. 4, pp. 2946-2957, 2023.

[15] H. Bahramiabarghouei, E. Porter, A. Santorelli, B. Gosselin, M. Popović, and L. A. Rusch, "Flexible 16 antenna array for microwave breast cancer detection," *IEEE Transactions on Biomedical Engineering,* vol. 62, no. 10, pp. 2516-2525, 2015.

[16] A. Hossain, M. T. Islam, M. T. Islam, M. E. Chowdhury, H. Rmili, and M. Samsuzzaman, "A planar ultrawideband patch antenna array for microwave breast tumor detection," *Materials,* vol. 13, no. 21, p. 4918, 2020.

[17] F.-e. Zerrad *et al.*, "Multilayered metamaterials array antenna based on artificial magnetic conductor's structure for the application diagnostic breast cancer detection with microwave imaging," *Medical Engineering & Physics,* vol. 99, p. 103737, 2022.

[18] M. N. Hamza *et al.*, "Low-cost antenna-array-based metamaterials for non-invasive early-stage breast tumor detection in the human body," *Biosensors,* vol. 12, no. 10, p. 828, 2022.

[19] HFSS: High Frequency Structure Simulator, ANSYS, Canonsburg, PA ,USA, Jan. 2024. [Online]. Available: http://www.ansys.com